Nat. Hazards Earth Syst. Sci. Discuss., 3, 2913–2952, 2015
www.nat-hazards-earth-syst-sci-discuss.net/3/2913/2015/
doi:10.5194/nhessd-3-2913-2015

Natural Hazards and Earth System Sciences
Discussions

Appraising the Early-est earthquake monitoring system for tsunami alerting at the Italian candidate Tsunami Service Provider

F. Bernardi[1], A. Lomax[2], A. Michelini[1], V. Lauciani[1], A. Piatanesi[1], and S. Lorito[1]

[1]Istituto Nazionale di Geofisica e Vulcanologia, Via di Vigna Murata 605, 00143 Roma, Italy
[2]ALomax scientific, Allé du Micocoulier 161, 06370 Mouans-Sartoux, France

Received: 16 March 2015 – Accepted: 16 March 2015 – Published: 30 April 2015

Correspondence to: F. Bernardi (fabrizio.bernardi@ingv.it)

Published by Copernicus Publications on behalf of the European Geosciences Union.

Abstract

.. and discuss the performance of…

In this paper we present the procedure for earthquake location and characterization implemented in the Italian candidate Tsunami Service Provider at INGV in Roma. Following the ICG/NEAMTWS guidelines, the first tsunami warning messages are based only on seismic information, i.e. epicenter location, hypocenter depth and magnitude, which are automatically computed by the software Early-est. Early-est is a package for rapid location and seismic/tsunamigenic characterization of earthquakes. The Early-est software package operates on offline-event or continuous-realtime seismic waveform data to perform trace processing and picking, and, at a regular *report interval*, phase association, event detection, hypocenter location, and event characterization. In this paper we present the earthquake parameters computed by Early-est from the beginning of 2012 till the end of December 2014 at global scale for events with magnitude $M \geq 5.5$, and the detection timeline. The earthquake parameters computed automatically by Early-est are compared with reference manually revised/verified catalogs. From our analysis the epicenter location and hypocenter depth parameters do not differ significantly from the values in the reference catalogs. The epicenter coordinates generally differ less than 20 ∓ 20 km from the reference epicenter coordinates; focal depths are less well constrained and differ generally less than 0 ∓ 30 km. Early-est also provides mb, M_{wp} and M_{wpd} magnitude estimations. mb magnitudes are preferred for events with $M_{wp} \lesssim 5.8$, while M_{wpd} are valid for events with $M_{wp} \gtrsim 7.2$. The magnitude mb show wide differences with respect to the reference catalogs, we thus apply a linear correction $mb_{corr} = mb \cdot 0.52 + 2.46$, such correction results into $\delta mb \approx 0.0 \mp 0.2$ uncertainty with respect the reference catalogs. As expected the M_{wp} show distance dependency. M_{wp} values at stations with epicentral distance $\Delta \lesssim 30^{\circ}$ are significantly overestimated with respect the CMT-global solutions, whereas M_{wp} values at stations with epicentral distance $\Delta \gtrsim 90^{\circ}$ are slightly underestimated. We thus apply a 3rd degree polynomial distance correction. After applying the distance correction, the M_{wp} provided by Early-est differs from CMT-global catalog values of about $\delta M_{wp} \approx 0.0 \mp 0.2$. Early-est con-

tinuously acquires time series data and updates the earthquake source parameters. Our analysis shows that the epicenter coordinates and the magnitude values converge rather quickly toward the final values. Generally we can provide robust and reliable earthquake source parameters to compile tsunami warning message within less than about 15 min after event origin time.

1 Introduction

Tsunamis may produce dangerous coastal flooding and inundations accompanied by powerful currents which can cause significant damage and casualties. A tsunami may be generated when an large or great earthquake occurs in sea areas or inland close to the coast. When such earthquakes occur, a tsunami warning should be issued to alert national authorities and emergency management officials to take actions for the entire tsunami hazard zone and to evacuate the population and/or to secure critical facilities such as nuclear power plants. In the presence of evacuation plans, prepared in advance, and of well-trained communities, tsunami warnings could be also sent directly to the population.

Reliable tsunami warnings should be disseminated as fast as possible in order to be effective also for the coastal areas very close to the earthquake source, since a tsunami may arrive at these areas very soon after the event origin time. Population exposed to tsunami hazard in the near field of the source, however, should be aware that the time between warning issuance and tsunami impact may be too short to escape the tsunami, that warning may arrive even after the tsunami, or the system may be subject to failure, for several reasons. Hence, they should also be trained to self-evacuate relying, when present, on natural warnings, such as strong and/or unusually long shaking, sea withdrawal, anomalously rising tide, roaring sounds from the sea, etc.

To provide the earliest possible alerts initial warnings from regional tsunami warning systems are normally based only on seismic information. Thus, fast, precise and reliable earthquake source parameters like epicenter coordinates, hypocenter depth and

magnitude are crucial for seismologically based tsunami early warning procedures. This is particularly important in the Mediterranean Sea, where offshore tsunami sensors are not in place.

The Istituto Nazionale di Geofisica e Vulcanologia (INGV) in Italy is a candidate Tsunami Service Provider (cTSP) in the framework of ICG/NEAMTWS (NEAMTWS, 2011), which is the tsunami early warning and mitigation system established by IOC/UNESCO for the North-eastern Atlantic, the Mediterranean and connected seas. For this reason, the Centro Allerta Tsunami (CAT) (tsunami alert centre in Italian), has been established at the INGV headquarter in Rome at the end of 2013. The CAT mission is to implement and maintain a 24/7 service along with the ordinary seismic surveillance of the national territory, and to work towards a Probabilistic Tsunami Hazard Assessment (PTHA) for the italian coasts, for seismically-induced tsunamis (Basili et al., 2013; Lorito et al., 2015). CAT-INGV started operations on a 24/7 basis as cTSP in October 2014. Monthly communication tests are performed towards national authorities, subscriber IOC member states and other institutions, such as the DG-ECHO Emergency Response Coordination Center in Brussels. Further than INGV, in the NEAM region there are three more cTSPs, which already started to operate. They are CENALT in France, NOA in Greece, and KOERI in Turkey. IPMA, in Portugal, should start soon. Each of them have its specific competence source areas within the NEAM region.

At the national level, INGV is responsible of issuing messages to the Civil Protection authority, which is presently responsible for alert dissemination. INGV also maintains the national seismic network and exchanges seismic data in real time with a number of international seismic data providers. The Istituto Superiore per la Protezione e Ricerca Ambientale (ISPRA) maintains the national sea level network and provides real time data to INGV monitoring room. The implemented tsunami warning procedure uses the *Early-est* software developed by Lomax and Michelini (2009a, b, 2011, 2012) to rapidly locate and determine the magnitude for large to great regional and teleseismic earthquakes.

The purpose of this paper is to analyze the Early-est performances regarding past events, in order to evaluate its reliability for the near-real time tsunami warnings disseminated by the INGV, and eventually tune the procedure as a whole.

INGV cTSP follows the ICG/NEAMTWS guidelines. ICG/NEAMTWS rules establish that a cTSP must disseminate a tsunami message, with warning levels that depend on location, magnitude and depth of the earthquake according to a decision matrix, for all earthquakes with magnitudes $M \geq 5.5$ in their zone of competence. Messages are sent for earthquakes that are large and shallow enough, and occurring in sea areas or inland but sufficiently close to the coast to likely generate a tsunami. INGV competence source zone extends from Gibraltar Strait to the west, to Marmara and Levantine Seas to the east.

The seismicity in the Mediterranean region is moderate to high, ~~but~~ including also M8+ earthquakes which occurred in the past generated significant tsunamis (Maramai et al., 2014; Lorito et al., 2015). It is difficult to assess if M9-class earthquakes might occur, which can not be excluded (Kagan and Jackson, 2013). Even if tsunamigenic earthquakes are likely to occur, their time recurrence intervals are however quite long (Koravos et al., 2003; Jenny et al., 2004; Bungum and Lindholm, 2007); moreover, the Mediterranean Sea is a relatively small area, and earthquakes with $M \geq 5.5$ do not occur very frequently. Early-est has been now running for several years, but only since the beginning of March 2012 has its current major version release been online and its solutions could be systematically archived. Thus we do have few events to analyze for tuning our tsunami alert procedure (Table 1). For this reason we perform our analysis using all worldwide occurred earthquakes located by Early-est since March 2012. To perform the analysis and tune our procedure we proceed by comparing the epicenters, the hypocenter depths and magnitudes estimation provided fully automatically by Early-est with the same parameters provided by other agencies taken as reference. Such agencies provide manually validated/revised locations and magnitude estimations for earthquakes at global scale.

This paper is structured as follows. In the next section, we briefly overview the Early-est algorithm. In Sect. 3 we describe the dataset used in our analysis. In the following three sections we then analyze and compare the earthquake source parameters provided by Early-est with the ones provided by the reference agencies; first the epicenter location (Sect. 4), then the hypocenter depth (Sect. 5) and last the magnitude (Sect. 6). In Sect. 7 we will analyze the speed performances of Early-est with respect the location and the magnitude parameters in order to set the timeline of our automatic tsunami warning procedure. Last the the discussions and conclusions.

2 Early-est algorithm description

Early-est is a software package for rapid location and seismic/tsunamigenic characterization of earthquakes. The Early-est software package operates on offline-event or continuous-realtime seismic waveform data to perform trace processing and picking, and, at a regular *report interval*, phase association, event detection, hypocenter location, and event characterization. This characterization (Table A1) includes mb and M_{wp} magnitudes, the determination of apparent rupture duration, T_0, large earthquake magnitude, M_{wpd}, and assessment of tsunamigenic potential using T_d and T_{50}Ex, as described in Lomax and Michelini (2009a, b, 2011). The Early-est program reads mini-seed data packets from file or a SeedLink server (http://ds.iris.edu/ds/nodes/dmc/services/seedlink, http://www.seiscomp3.org/wiki, doc/applications/seedlink), and passes each packet to a *trace-processing* module. The program also calls an *associate/locate* - reporting module at regular *reporting intervals* (e.g. after all data is read for mini-seed; every 1 min for SeedLink). The Early-est software maintains a persistent *pick list* for the current *reporting window* (e.g. the last hour before real-time) and an *event list* for a specified archive interval (e.g. the last 10 days). The *pick list* is updated continuously as picking and trace processing are applied to new data packets. The *event list* is updated at each *reporting interval* as new event locations are found or previous locations are deleted. At each *reporting interval* the *associate/locate* module

processes the current *pick list* from scratch, without making use of previous associations or location information from the *event list*; this memory-less procedure simplifies the *associate/locate* module and makes it very robust with respect to changes in the *pick list*, but increases the computational load. To reduce this load, the persistence of association and location information for well located events is currently being added to Early-est.

2.1 Trace-processing module

The *trace-processing* module processes each new data packet passed by the Early-est program. This processing includes channel identification, quality control, filtering for picking, picking and further filtering and pre-processing as required for seismic and tsunamigenic event characterization (Table A1).

Picking in Early-est is performed by *FilterPicker* (Lomax et al., 2012; Vassallo et al., 2012), a general purpose, broad-band, phase detector and picker which is applicable to real-time seismic monitoring and earthquake early-warning. *FilterPicker* uses an efficient algorithm which operates stably on continuous, real-time, broadband signals, avoids excessive picking during large events, and produces onset timing, realistic timing uncertainty, onset polarity and amplitude information. In practice, it operates on a pre-defined number of frequency bands by generating a set of band-passed time-series with different center frequencies. Characteristic functions are determined for each frequency band and a pick is declared if and when, within a window of predefined time width, the integral of the maximum of the characteristic functions exceeds a pre-defined threshold.

After picking on each new data packet, for each pick in the *pick list* for the current packet channel, the *trace-processing* module applies various analyses on the channel data and updates values needed for event characterization. Recursive, time-domain algorithms are used for all filtering and other time-series processing.

2.2 Associate/locate – reporting module

The Early-est *associate/locate – reporting* module calls an *oct-tree associate/locate* module with the current *pick list*, and then the *reporting module* which determines event characterization results and generates graphical and alpha-numeric reporting output. The *oct-tree associate/locate* module efficiently and robustly associates picks, and detects and locates seismic events over the whole Earth from 0 to 700 km depth using the efficient, non-linearized, probabilistic and global, oct-tree importance-sampling search (Lomax and Curtis, 2001; Lomax et al., 2009). The objective function for the oct-tree search is a probability function, $P(\boldsymbol{x})$, based on stacking of implicit origin-times for each pick for each potential source $\boldsymbol{x}_{\text{test}}$: given a seismic wave velocity model (currently ak135; Kennett et al., 1995), a pick time tp at a seismic station, and assuming a seismic phase type that may have produced the pick, the phase travel-time from source xtest to station T_x can be calculated and thus the implicit origin-time T_0 for the source and phase can be determined by back projection (e.g., $T_0 = t_p - T_x$). The set of stacks of T_0 for all picks forms a histogram over potential origin-times for a source at $\boldsymbol{x}_{\text{test}}$. If the maximum histogram value exceeds a specified threshold, and if the associated picks for the maximum pass tests on amplitudes and station distributions, then $P(\boldsymbol{x}_{\text{test}})$ is retained to drive further the oct-tree search to find a maximum $\boldsymbol{x}_{\text{max}} = \max[P(\boldsymbol{x})]$ and define a seismic event at $\boldsymbol{x}_{\text{max}}$ and associated picks. See Appendix for more details.

The Early-est *reporting* module processes the current *pick list* and *event list* to determine event characterization results (Table A1) and generate graphical, alpha-numeric, XML, HTML and other reporting output for events, picks, stations, etc. An e-mail or other alert message can be generated for each event with magnitudes or tsunamigenic potential exceeding pre-set thresholds. Figure A1 shows the main graphical display of Early-est, which summarizes the evolving trace-processing, associate/locate and event characterization results in real-time.

3 Dataset

The Early-est catalog (EEc in this paper) includes fully automatic and unrevised location and magnitude estimations for 5449 global regional and teleseismic events occurred with magnitude $M \gtrsim 5.0$. The current major version release of Early-est runs since the beginning of March 2012. Our analysis will use locations and magnitudes for events occurred from the begin of March 2012 till end of December 2014; later events are not considered in this work. ~~Early-est uses waveforms from hundreds of broadband seismic stations distributed worldwide.~~ At the beginning of March 2012 Early-est was using about 300 seismic broadband stations. The number of stations has been continuously increasing, and at the end of September 2014 the Early-est software ~~has~~ was using a virtual station network of 494 stations (Fig. 1).

We use the following as *reference catalogs*: (i) the catalog provided by the Deutches GeoForschungsZentrum (Gc in this paper), (ii) the catalog provided by the National Earthquake Information Center (Nc in this paper), (iii) the catalog provided by the EMSC-CSEM (Cc in this paper), (iv) the catalog provided by Global CMT (CMTc in this work), (v) and the catalog provided by the Pacific Tsunami Warning Center (Pc in this paper). The CMTc and the Pc will be used specifically to compare and assets the M_{wp} and M_{wpd} magnitudes.

The above mentioned observatories and centers provide earthquake source parameters for different time windows. All location coordinates, hypocenter depth and magnitude estimations from these reference catalogs are manually verified and/or revised. Table 2 summarizes the catalogs abbreviations and time windows for each catalog used in this work. The ICG/NEAMTWS guidelines indicate that tsunami warning must be disseminated for all events in the Mediterranean and Northen-eastern Atlantic regions with $M \geq 5.5$. For this reason, although Early-est locate events with magnitude $M \gtrsim 5.0$, our analysis will focus only on worldwide earthquakes with magnitude $M \geq 5.5$.

4 Epicenter

In this section we use the three reference catalogs Nc, Gc, and Cc and the Early-est catalog EEc.

We first build three couples with the three reference catalogs (Gc-Cc, Cc-Nc and Gc-Nc) and we compute the distance between the epicenter coordinates for each earthquake listed in both catalogs of each couple.

The top panel in Fig. 2 shows the histograms representing the distributions of the location differences in each couple of the reference catalogs. The $M \geq 5.5$ earthquakes are generally located with a mean distance uncertainty smaller than $\overline{\delta\Delta_{ref}} \lesssim 20 \mp 25$ [km]; almost 95 % of all earthquakes are located with distance differences $\delta\Delta_{ref} \lesssim 50$ [km]. We did not find evidences for geographical and/or tectonic dependence of this uncertainty.

We then compare the epicenter coordinates between the earthquakes listed into the EEc and in each of the three reference catalogs (Fig. 2, bottom panels), i.e. we build the couples EEc-Cc, EEc-Nc and EEc-Gc. The histograms show that the epicenter location differences between the EEc and the reference catalogs $\delta\Delta_{EEc}$ are similar to the differences plotted on the top panels. The mean location differences between the EEc and the reference catalogs is about $\overline{\delta\Delta_{EEc}} \lesssim 20 \mp 20$ [km] and 95 % of all events into the dataset show differences $\delta\Delta_{EEc} \lesssim 45$ [km].

5 Hypocenter depth

In this section we proceed as described in the section above: we use the three reference catalogs Nc, Gc, and Cc and the Early-est catalog EEc and to build the catalog couples used in the previous Sect. 4. We then compute the depth difference between the hypocenters for each earthquake listed in both catalogs of each couple.

Figure 3 (top panels) shows the histograms representing the distribution of the depth differences in each couple of the reference catalogs. The hypocenter depth estimation for earthquakes with magnitude $M \geq 5.5$ listed into global catalogs is generally well

resolved: the mean and SD difference are $\overline{\delta Z_{\text{ref}}} \approx 0 \mp 25$ [km] for all catalog couples. We did not found evidences for geographical and/or tectonic dependence of this uncertainty.

We then compare the hypocenter depths between the EEc and each of the three reference catalogs (Fig. 3 bottom panels, couples EEc-Cc, EEc-Nc and EEc-Gc). The bottom panels show that the hypocenter depth estimation differences between the Early-est catalog and the reference catalogs do not differ significantly: the mean difference distributions are about $\overline{\delta Z_{\text{EEc}}} \approx 0 \mp 30$ [km].

6 Magnitude

Early-est provides three different types of magnitude: mb, M_{wp} and M_{wpd} (Lomax and Michelini, 2011) and then automatically decides each minute which magnitude type is the most significant following the rules in Table 3. The criteria to assign the *best magnitude* listed in Table 3 follow two simple principles: (i) a minimum number of observations is required to obtain reliable magnitude estimations, and (ii) magnitude types are reliable within magnitude ranges. Following Lomax and Michelini (2009a, b, 2011) we set the validity range $5.8 \leq M_{\text{wp}} < 7.2$ for the *best magnitude*; mb is assigned to *best magnitude* when $M_{\text{wp}} < 5.8$ and M_{wpd} is assigned to *best magnitude* when $M_{\text{wp}} > 7.2$ In this work we compare the Early-est magnitude types M_{wp} and M_{wpd} with respect to the reference magnitude types M_{wp} and M_{w}, since M_{wp} should be considered proportional and equivalent to M_{w}, and M_{wpd} equivalent to M_{wp} respectively but for $M_{\text{wp}} \geq 7.2$. Since the ICG/NEAMTWS guidelines indicate that for earthquakes with hypocenter depth $Z > 100$ [km] should be delivered a unique general warning for all events with $M \geq 5.5$, in this section we analyze the magnitudes results only for events with $Z \leq 100$ [km].

As in Sects. 4 and 5 we first compare the magnitudes provided by the reference catalogs. Then, we compare the magnitudes provided by Early-est with the magnitudes listed ~~in~~to the reference catalogs. First we will compare all *best magnitude* (i.e. mb or

M_{wp}) together, considering only the couple between catalogs where the magnitude types are identical (Fig. 4). This comparison will provide a general overview on how the *best magnitude* of Early-est matches with the magnitude of the reference catalogs.

Figure 4 shows the distribution of the magnitude differences $\delta M^{\text{EEc}} = M^{\text{EEc}} - M^{\text{ref}}$ between the values of the EEc and the ones of the reference catalogs (Nc and Cc, since the Gc catalog do not provide the magnitude type).

Such narrow and well centered to the distribution does not appear when comparing the Early-est magnitudes with the magnitudes of the two reference catalogs (center and right panels of Fig. 4). When comparing the Early-est magnitudes with the magnitudes of the two reference catalogs (center and right panels of Fig. 4), Early-est seems to overestimate the magnitudes of about $\overline{\delta M^{\text{EEc}}} \approx 0.1 \mp 0.2$. The percentiles show that more than 10 % of the magnitudes provided by Early-est differ significantly from the magnitude provided by the reference catalogs. The overestimation and the wider distribution appear to be homogeneously distributed among all magnitude ranges.

In the next subsections we will analyze more in details the magnitude values for each single magnitude type mb and M_{wp} separately.

6.1 mb

In this subsection we compare the mb^{EE} magnitudes provided by Early-est with respect the mb magnitudes provided by Neic (mb^{Nc}) and EMSC (mb^{Cc}). We use the mb^{EEc} only when Early-Est assigns best magnitude = mb following the rules of Table 3.

Figure 5 shows the mb^{EEc} with respect to the mb^{Nc} (top left panel) and with respect to the mb^{Cc} (top right panel). These two plots show sparse distributed values, which are coherent with the magnitude differences of the histograms in Fig. 5c and d. The mean $\overline{\delta \text{mb}}$ indicates that the catalogs are coherent, but the SD and the percentiles point out that the mb^{EEc} can be significantly underestimated or overestimated with respect mb^{Nc} and mb^{Cc}.

In order to correct such sparse distributions we computed a linear regression function for each panel (thick dashed lines on the top panels). These functions are computed for $f_1 = \mathrm{mb}^{\mathrm{EEc}} \rightarrow \mathrm{mb}^{\mathrm{Nc}}$ and for $f_2 = \mathrm{mb}^{\mathrm{EEc}} \rightarrow \mathrm{mb}^{\mathrm{Cc}}$ respectively – the constant a and b of the linear function are showed in the left upper corners of Fig. 5a and b. We then applied the regression functions f_1 and f_2 to the $\mathrm{mb}^{\mathrm{EEc}}$ values and we recompute the differences (third row of histograms). Both new distributions have mean values close to 0 and smaller SD and percentiles with respect the original ones.

The two functions appear similar but show different a and b constants. In order to test if such differences are significant, we applied the first function f_1, derived for $\mathrm{mb}^{\mathrm{EEc}} \rightarrow \mathrm{mb}^{\mathrm{Nc}}$, and we computed the differences with respect the $\mathrm{mb}^{\mathrm{Cc}}$ values. Second we applied function f_2 derived for $\mathrm{mb}^{\mathrm{EE}} \rightarrow \mathrm{mb}^{\mathrm{Cc}}$ and computed the residuals with respect the $\mathrm{mb}^{\mathrm{Nc}}$ values. Applying these corrections we obtain two new difference distributions $\delta\mathrm{mb}_{\mathrm{Cc}}^{\mathrm{EEc}\rightarrow\mathrm{Nc}}$ and $\delta\mathrm{mb}_{\mathrm{Nc}}^{\mathrm{EE}\rightarrow\mathrm{Cc}}$ (bottom left and right panels). The distributions $\delta\mathrm{mb}^{\mathrm{EE}\rightarrow\mathrm{Nc}}$ and the $\delta\mathrm{mb}_{\mathrm{Cc}}^{\mathrm{EEc}\rightarrow\mathrm{Nc}}$, and the distributions $\delta\mathrm{mb}^{\mathrm{EE}\rightarrow\mathrm{Cc}}$ and the $\delta\mathrm{mb}_{\mathrm{Nc}}^{\mathrm{EE}\rightarrow\mathrm{Cc}}$ as well, appear to be significantly different. We performed a t test between $\delta\mathrm{mb}^{\mathrm{EE}\rightarrow\mathrm{Nc}}$ and the $\delta\mathrm{mb}_{\mathrm{Cc}}^{\mathrm{EEc}\rightarrow\mathrm{Nc}}$ distribution and between $\delta\mathrm{mb}_{\mathrm{Cc}}^{\mathrm{EEc}\rightarrow\mathrm{Nc}}$ and $\delta\mathrm{mb}_{\mathrm{Nc}}^{\mathrm{EEc}\rightarrow\mathrm{Cc}}$. The null hypotheses H_0 is rejected at more than 95 %.

From the percentiles of the corrected distributions, particularly on the left side, we observe that the regression function f_1, when applied, produces a narrower magnitude difference distribution with respect the function f_2. After applying the linear corrections, the resulting $\mathrm{mb}^{\mathrm{EE}}$ uncertainty is about $\nu \approx 0.00 \mp 0.14$. ??

6.2 M_{wp}

As a reference, we first compare the magnitudes $M_{\mathrm{wp}}^{\mathrm{Pc}}$ values provided by the Pacific Tsunami Warning Center (PTWC) using the correction of Whitmore et al. (2002) with the $M_{\mathrm{w}}^{\mathrm{CMTc}}$ of the CMT-Harvard catalog (Fig. 6). The magnitudes compare well with

a mean difference $\mu = 0.04 \mp 0.19$ for events with magnitude about $M_{\mathrm{wp}} \lesssim 7.0$–$7.5$. For larger events, the magnitudes $M_{\mathrm{wp}}^{\mathrm{Pc}}$ begin to overestimate with respect to the $M_{\mathrm{w}}^{\mathrm{CMTc}}$.

We now compare the magnitudes $M_{\mathrm{wp}}^{\mathrm{EEc}}$ with the $M_{\mathrm{w}}^{\mathrm{CMTc}}$ (Fig. 7). The $M_{\mathrm{wp}}^{\mathrm{EEc}}$ magnitudes appear to be significantly overestimated, particularly for earthquakes with $M_{\mathrm{w}}^{\mathrm{CMT}} \leq 6.5$.

M_{wp} is based on the far-field approximation to the P wave displacement due to a double couple point source (Tsuboi et al., 1995), thus we should consider that M_{wp} computed in the near field may result biased. In fact Hirshorn et al. (2012) showed that single station M_{wp} values measured at stations at epicentral distances $\Delta \leq 15^{\circ}$ have positive residuals with respect the Harvard centroid moment tensor M_{w}. Nevertheless, our procedure is built to obtain reliable M_{wp} estimates as fast as possible, thus we aim to also use M_{wp} measured from stations close to the epicenter.

To test if our $M_{\mathrm{wp}}^{\mathrm{EEc}}$ values may be dependent as a function of the distance between station and epicenter, we plotted the station residuals at each station for each event with respect the epicenter distance (Fig. 8). Station residuals are defined as $\delta M_{\mathrm{wp}}^{i} = M_{\mathrm{wp}}^{\mathrm{EEc},i} - M_{\mathrm{w}}^{\mathrm{CMTc}}$, where i indicate the M_{wp} values measured at each station.

Figure 8 top left shows the residuals $\delta M_{\mathrm{wp}}^{i}$ (grey dots) for all events with hypocenter depth ≤ 100 [km] plotted with respect the epicentral distance in degrees. From these residuals we compute the regression function (dashed line in Fig. 8):

$$f(\Delta) = -1.32e^{-6} \cdot \Delta^3 + 2.40e^{-4} \cdot \Delta^2 - 0.0146 \cdot \Delta + 0.314 \quad (1)$$

Figure 8 and Eq. (1) show, that the $\delta M_{\mathrm{wp}}^{i}$ are overestimated for distances $\Delta \lesssim 30^{\circ}$ and slightly underestimate for distances $\Delta \gtrsim 90^{\circ}$. After applying the regression function $f(\Delta)$ to the station values, the distance dependency of M_{wp}^{i} is removed (Fig. 8 top right panel).

The distance dependency of the measured $M_{\mathrm{wp}}^{\mathrm{EEc},i}$ at each station reflects into a general overestimation of the $M_{\mathrm{wp}}^{\mathrm{EEc}}$ with respect the $M_{\mathrm{w}}^{\mathrm{CMTc}}$ (Fig. 7 bottom left). The overestimation of $M_{\mathrm{wp}}^{\mathrm{EEc}}$ could of course be removed using only M_{wp} measured at stations

with epicentral distance $30^{\circ} \leq \Delta \leq 90^{\circ}$. Nevertheless Early-est is designed to provide automatic magnitude estimations within few minutes after event origin time in order to disseminate early tsunami warnings. Thus the closer stations are relevant and must be used.

For this reason we apply the Eq. (1) to remove the distance dependency of the measured $M_{wp}^{EEc,i}$ and we then recompute the magnitude events $M_{wp,\,corr}^{EEc}$. To recompute the $M_{wp,\,corr}^{EEc}$ we follow the Early-est procedure: we trim off stations with $M_{wp}^{EEc,i} <$ 10th percentile and with $M_{wp}^{EEc,i} >$ 10th percentile. The event magnitude is M_{wp} = 50th percentile of the remaining values. The histogram of Fig. 8 bottom right shows the corrected magnitude differences $\delta M_{wp,\,corr}^{EEc}$. The right side shift of the original magnitude differences distribution (Fig. 8 bottom left) is corrected. The resulting magnitude M_{wp}^{EEc} uncertainty with respect the M_{w}^{CMTc} is $\delta M_{wp} = 0.0 \mp 0.2$, which consistent with the uncertainty of the M_{wp} provided by the with PTWC with respect the global CMT-Harvard catalog.

7 Speed performances and tsunami warning alert timeline

In the previous section we analyzed the final epicenter location, hypocenter depth and magnitude values provided by Early-est, i.e. the values obtained about 20 min to one hour after event origin time. However, a tsunami alert can provide useful warning be only if delivered within a short time after event origin time and with reliable earthquake source parameters. In order to plan the timeline procedure at the CAT-INGV, we want to know how fast the earthquake source parameters computed by Early-est converge toward the final values.

We thus first analyze how fast Early-est provides a first automatic location, and second how fast the epicenter coordinates and the magnitudes stabilize toward the final values.

The histogram in Fig. 9 shows the delay time after event origin time when a first automatic location of Early-est becomes available using the station coverage of Fig. 1.

We generally have to wait at least two minutes in order to have a first automatic solution; within 7 and 10 min after event origin time about the 95 % and the 100 % respectively of all earthquakes are located. At global scale a large number of earthquakes are located along the oceanic ridges and trenches, which are far away from most of the seismic stations. In the Mediterranean area the distances between earthquake and seismic stations are generally shorter than at global scale. Table 1 lists the 12 events with magnitude $M \geq 5.5$ occurred in the Mediterranean area between March 2012 and the end of December 2014. These 12 events do not allow to build a reliable statistic, but from Table 1 we may reasonably expect to locate an event in the Mediterranean area with magnitude $M \geq 5.5$ within 2–3 min after event origin time.

In order to disseminate reliable tsunami warnings, we need also reliable event source parameters. Figure 10 shows how fast a first location (top panel) and magnitude (bottom panel) are obtained.

Both panels indicate that for most of the events the epicenter coordinates and magnitudes within the first 8–10 min after the first available location may be considered stable and significantly close to the final values, since the magnitudes are $\mu + \sigma \leq 0.1$ and the epicenter locations are $\mu + \sigma \leq 10$ [km] respectively.

The CAT-INGV uses the earthquake source parameters provided by Early-est to compile the tsunami warning message to disseminate to the civil authorities. The mission of the CAT is to provide tsunami warnings for earthquakes with $M \geq 5.5$ which occur in the Mediterranean reagion according to the ICG/NEAMTWS guidelines.

Based on the speed performances of Early-Est on computing reliable earthquake source parameters (Fig. 10) and on the minimum delay time after event origin time to locate and estimate the magnitude of an event in the Mediterranean (Table 1), we set a timeline that allows the CAT-INGV to compile and distribute reliable tsunami warning messages within the very short but reasonable time interval after event origin time.

Our procedure compiles automatically a tsunami warning alert message for the 2nd, the 5th and the 8th locations available. Considering that the first location in the Mediterranean area may be available within 2–3 min after event origin time, the 2nd, the 5th

and the 8th locations are expected to be available between about 5, 8 and 11 min after event origin time. ~~In case of an earthquake~~ Therefore, in case of an earthquake in the Mediterranean area, the continuous monitoring of Early-est provides the relevant information to the seismologists for issuing tsunami warnings within about 15 min after event origin time.

8 Discussions and final remarks

From our analysis the automatic locations and source depth estimates provided by Early-est for global $M \geq 5.5$ earthquakes are robust and reliable, and the epicenter source parameter~~s~~ estimates by Early-est are coherent with the epicenter source parameters provided after manual revision/validation by other agencies (NEIC, GFZ and CSEM-EMSC) that locate earthquakes at global scale.

Generally our analysis showed that earthquakes with $M \geq 5.5$ can be located, when using seismic data form global networks, with a empirical uncertainty of about $v \approx 20 \mp 25$ [km]. The location provided by Early-est show similar uncertainty when compared to the other reference catalogs ($v \approx 20 \mp 25$ [km]).

The mean Early-est focal depth uncertainty for global $M \geq 5.5$ earthquakes is about $v \approx 0 \mp 25$ [km], which is also coherent with the focal depth uncertainty of the reference catalogs.

The fact that Early-est uses only a sub set of all worldwide public real-time station, and the fact that sometimes such number may be smaller because of latencies, does not seems to affect significantly the quality of the estimated epicenter coordinates and hypocenter depth.

The Magnitude is a key earthquake parameter to determine the tsunami alert level (see Sect. 1). The decision matrix defined by the NEAMTWS (2011) sets the tsunami warning level on the basis of the magnitude, hypocenter depth and of the distance between the epicenter and the coastal forecast points. The automatic magnitudes mb and M_{wp} provided by Early-est show differences with respect to the used reference

values that in some cases may be significant from the point of view of the tsunami warning perspective.

The magnitudes mb provided by Early-est compare well with the mb values provided by reference agencies from the point of view of the mean differences, but show sparse distribution that can be larger than ∓ 0.3 units of magnitude. Such sparse distribution can be corrected by increasing the signal-to-noise ratio threshold for the mb station values. On the other hand a higher signal-to-noise ratio threshold may reduce the number of station readings, and would require more stations to obtain a reliable mb value. This would result into a slower magnitude estimation, which may affect the efficiency and the speed required for tsunami warnings dissemination. A linear correction of the computed mb values produces indeed a reduction of the SD to about ∓ 0.15 units of magnitude. From our analysis, with the correction function f_1 we obtain more coherent mb values than with respect the correction function f_2 (Fig. 5).

Nevertheless the magnitude mb starts to saturate from magnitude mb$\gtrsim$6.0 and for this reason Early-est does not use mb when $M_{wp} \geq 5.8$. Thus, mb values apply to earthquakes which are not generally expected to be tsunamigenic. In these cases, however, the decision matrix (NEAMTWS, 2011) assigns an “advisory level” message in the near-field.

The Early-est magnitude M_{wp} values are reliable when computed using only stations with epicentral distance $30^\circ \leq \Delta \leq 90^\circ$. As expected ~~from~~ (Tsuboi et al., 1995; Hirshorn et al., 2012), single stations M^i_{wp} measurements at distance $\Delta \leq 30^\circ$ are significantly overestimated (Fig. 8). The observed distance dependent bias at each station results in a general overestimation of the final M_{wp} (Fig. 7). Early-est is designed to provide automatic magnitude estimation within few minutes after event origin time in order to disseminate early tsunami warning, thus the closer stations are relevant and must be used. For this reason we prefer to correct the station M_{wp} values to remove the overestimation of the single station M_{wp} values at distances $\Delta \leq 30^\circ$, instead of introducing a minimum distance cut off.

Since the assignment rules for the *best magnitude* depends on the number of station measuring reliable mb, M_{wp} and on M_{wpd} and the magnitude value for each ones (Table 3), the assigned *best magnitude* may vary between mb, M_{wp} and M_{wpd} at each run. This is particularly true within the first minutes after event origin time, when the number of available waveforms may still be small, and the magnitudes values may not be stable yet (Fig. 10). The linear correction for mb and the distance dependent correction for M_{wp} will thus produce a stable and reliable *best magnitude* useful for seismologically based tsunami early warning procedures.

Early-est is able to provide first location within about 7 min from origin time for almost 95 % of all worldwide earthquakes. In the Mediterranean area, where the epicentral distance between earthquake and seismic station is smaller, we may expect a first automatic location within 2–3 min after event origin time. Generally within less than 10 min after the first location, the estimations converge to the final and stable values.

The CAT-INGV provides seismologically based tsunami early warning when earthquakes with magnitude $M \geq 5.5$ occurs in the Mediterranean area. Such tsunami warning messages are based on the fully automatically location and magnitude estimations provided by the Early-est software. The analysis of a data-set of three years of worldwide earthquakes, showed that Early-est is a robust, reliable and efficient software for automatic real-time earthquake source parameter estimation, which provides reliable and robust location parameters and magnitude estimations within few minutes after event origin time.

Appendix: Oct-tree associate/locate module

The oct-tree associate/locate module (Fig. A2) efficiently and robustly associates picks, and detects and locates seismic events over the whole Earth from 0 to 700 km depth using the efficient, non-linearized, probabilistic and global, oct-tree importance-sampling search (Lomax and Curtis, 2001; Lomax et al., 2009). The objective function for the oct-tree search is a probability function, $P(\boldsymbol{x})$, based on stacking of implicit origin-times for

each pick for each potential source $\boldsymbol{x}_{test}$: given a seismic wave velocity model (currently ak135 Kennett et al., 1995), a pick time t_p at a seismic station, and assuming a seismic phase type that may have produced the pick, the phase travel-time from source $\boldsymbol{x}_{test}$ to station $T_{\boldsymbol{x}}$ can be calculated and thus the implicit origin-time T_0 for the source and phase can be determined by back projection (e.g., $T_0 = T_{\mathbf{p}} - T_x$). The set of stacks of T_0 for all picks forms a histogram over potential origin-times for a source at $\boldsymbol{x}_{test}$. If the maximum histogram value exceeds a specified threshold, and if the associated picks for the maximum pass tests on amplitudes and station distributions, then $P(\boldsymbol{x}_{test})$ is retained to drive further the oct-tree search to find a maximum $\boldsymbol{x}_{max} = max[P(\boldsymbol{x})]$ and define a seismic event at $\boldsymbol{x}_{max}$ and associated picks.

The oct-tree search is *direct* and non-linearized – it does not involve linearization of the equations relating the pick times to the source location, and is global and *probabilistic* – it samples throughout the prior probability density function (PDF) for the seismic location problem. The search uses an initial, coarse, regular grid-search followed by recursive, octal sub-division and sampling of cells in three-dimensional, latitude/longitude/depth space to generate a cascaded, oct-tree structure of sampled cells. The oct-tree search produces approximate *importance-sampling* – the spatial density of sampled cells follows the objective function P.

For each latitude/longitude/depth cell of volume v visited by the oct-tree search, a histogram-like stack over implicit origin-times for first-arrival, P phases (currently Pg, P, Pdiff, PKPdf) for all picks in the *pick list* is constructed. Each origin-time value T_0 is assigned a distance and pick-quality weighted amplitude A between 0 and 1.0, and an uncertainty σ determined by the sum of half the maximum travel-time range across the cell volume with the travel-time and pick uncertainties. Each implicit origin-time is included in the origin-time stack with amplitude A using two step-function time-limits at $T_0 \mp \sigma$ inserted in time order. After all picks have been processed, the maximum of the origin-time stack is found by a systematic scan over the available time-limits; the use of step-function time-limits and time ordering makes this scan very fast. All picks whose origin time-limits overlap the stack maximum time are flagged as associated. The stack

value, combined with the variance of the implicit origin-times from all associate picks, is converted to a probability, $P(\boldsymbol{x}, v)$. If the maximum stack value exceeds a specified threshold (currently 4.5), and if the associated picks for the maximum pass tests on amplitude attenuation, and station distance and azimuth distributions, then $P(\boldsymbol{x}, v)$ is stored for use in the progression of the oct-tree search. If any of these conditions are not met, then the *oct-tree associate/locate* module returns, with a flag that no event has been associated. $P(\boldsymbol{x}, v)$ represents the relative probability that an event is located within a cell of volume v at position $\boldsymbol{x}$.

The oct-tree search to associate/locate is paused when the subdivided cells reach an adaptively determined, minimum size (e.g. ≤ 5 km for a location constrained by regional to globally distributed stations, ≤ 1 km for a location constrained by locally distributed stations); at this pause uncertainty measures (e.g. PDF scatter samples) on the association stage are generated. The oct-tree search and cell subdivision is then continued for a fixed number of samples (currently about 4600) to obtain a refined, precise location by fixing the associated phases to those corresponding to the maximum of the $P(\boldsymbol{x}, v)$ found in the association stage. The fixing of the associated phases is necessary for small cell sizes since a decreasing cell volume combined with the step-function limits on origin-time leads to a continuous reduction in $P(\boldsymbol{x}, v)$ values and eventual instability and non-convergence of the oct-tree search near and at the optimal source location. The precise oct-tree results provide uncertainty measures (e.g. PDF scatter samples, uncertainty ellipsoid) on the location.

When the *oct-tree associate/locate* module returns an event, the associated picks for this event are masked in the *pick list* and the *oct-tree associate/locate* module is called again using the remaining, non-associated picks, until no further events are returned. Thus multiple events can be associated and located within a report interval, and, in general, the events are identified in order of the number of associated picks and better location constraint.

Early-est runs the *oct-tree associate/locate* module every 1 min using all picks from the past hour, without knowledge of or preserving information from previously associa-

tions and event locations. This procedure makes Early-est relatively simple algorithmically and robust with regards to changes in the set of available picks and the number of associated picks defining locations. In particular, this procedure allows early stage locations with few associated picks to easily move in space or origin time, or to split into multiple events, or to be absorbed into other events, or to disappear as more pick data becomes available. However, this procedure is inefficient for later stage event locations which are defined by a larger number of associated picks, e.g. more than 10–20 picks, since such locations are very unlikely to change; much processing effort is repeated each minute to re-obtain a previous result. This inefficiency can be problematic after large earthquakes, when the repeated re-processing of hundreds of picks from a mainshock and large aftershock can cause Early-est to fall behind real-time.

Acknowledgements. The magnitude Mwp parameters of the Pc used in this paper were provided to the authors of this paper by the courtesy of Barry Hirshorn by the Pacific Tsunami Warning Center. We used broadband seismograms recorded by the Global Seismic Network obtained from the IRIS DMC and from NEIC. This work has been funded by the Italian Flagship Project RITMARE and by the EU FP7 project NERA (262330). The Early-est software is being further developed in the framework of the agreement between Italian DPC and INGV, annex B2 (2015). Figures were drawn using the Generic Mapping Tools (Wessel and Smith, 1995) and Matplotlib (Hunter, 2007).

References

Basili, R., Tiberti, M. M., Kastelic, V., Romano, F., Piatanesi, A., Selva, J., and Lorito, S.: Integrating geologic fault data into tsunami hazard studies, Nat. Hazards Earth Syst. Sci., 13, 1025–1050, doi:10.5194/nhess-13-1025-2013, 2013.

Bormann, P. and Saul, J.: The new IASPEI standard broadband magnitude mb, Seismol. Res. Lett., 79, 698–705, doi:10.1785/gssrl.79.5.698, 2008. 2940

Bormann, P. and Saul, J.: Earthquake magnitude, in: Encyclopedia of Complexity and Systems Science, edited by: Meyers, A., Springer, New York, 23 pp., 2473–2496, doi:10.1007/978-0-387-30440-3_151, 2009. 2940

Bungum, H. and Lindholm, C.: Tsunamigenic Seismic Sources in the North Sea, the Norwegian Continental Margin and the Norwegian-Greenland Sea, Tech. rep., NORSAR, ICG/NORSAR, Kjeller, Norway, 2007. 2917

Hardebeck, J. L. and Shearer, P. M.: A new method for determining first-motion focal mechanisms, B. Seismol. Soc. Am., 92, 2264–2276, 2002. 2940

Hirshorn, B., Weinstein, S., and Tsuboi, S.: On the application of M_{wp} in the near field and the March 11, 2011 Tohoku Earthquake, Pure Appl. Geophys., 170, 975–991, doi:10.1007/s00024-012-0495-3, 2012. 2926, 2930

Hunter, J. D. and Matplotlib: A 2D graphics environment, Computing, in: Science & Engineering, 9, 90–95, 2007.

Jenny, S., Goes, S., Giardini, D., and Kahle, H.-G.: Earthquake recurrence parameters from seismic and geodetic strain rates in the eastern Mediterranean, Geophys. J. Int., 157, 1331–1347, doi:10.1111/j.1365-246X.2004.02261.x, 2004. 2917

Kagan, Y. Y. and Jackson, D. D.: Tohoku Earthquake: a surprise?, B. Seismol. Soc. Am., 103, 1181–1194, doi:10.1785/0120120110, 2013. 2917

Kennett, B. L. N., Engdahl, E. R., and Buland, R.: Constraints on seismic velocities in the Earth from travel times, Geophys. J. Int., 122, 108–124, 1995. 2920, 2932

Koravos, G. C., Main, I. G., Tsapanos, T. M., and Musson, R. M. W.: Maximum earthquake magnitudes in the Aegean area constrained by tectonic moment release rates, Geophys. J. Int., 152, 94–112, 2003. 2917

Lomax, A. and Curtis, A.: Fast, probabilistic earthquake location in 3D models using oct-tree importance sampling, Geophys. Res. Abstr., 3, 2001. 2920, 2931

Lomax, A. and Michelini, A.: M_{wpd}: a duration-amplitude procedure for rapid determination of earthquake magnitude and tsunamigenic potential from P waveforms, Geophys. J. Int., 176, 200–214, doi:10.1111/j.1365-246X.2008.03974.x, 2009a. 2916, 2918, 2923, 2940

Lomax, A. and Michelini, A.: Tsunami early warning using earthquake rupture duration, Geophys. Res. Lett., 36, L09306, doi:10.1029/2009GL037223, 2009b. 2916, 2918, 2923, 2940

Lomax, A. and Michelini, A.: Tsunami early warning using earthquake rupture duration and P-wave dominant period: the importance of length and depth of faulting, Geophys. J. Int., 185, 283–291, doi:10.1111/j.1365-246X.2010.04916.x, 2011. 2916, 2918, 2923, 2940

Lomax, A. and Michelini, A.: Tsunami early warning within 5 min, Pure Appl. Geophys., 170, 1385–1395, doi:10.1007/s00024-012-0512-6, 2012. 2916, 2939

Lomax, A., Michelini, A., and Curtis, A.: Earthquake location, direct, global-search methods, in: Encyclopedia of Complexity and Systems Science, part. 5, 2449–2473, doi:10.1007/978-0-387-30440-3_150, 2009. 2920, 2931

Lomax, A., Satriano, C., and Vassallo, M.: Automatic picker developments and optimization: FilterPicker – a robust, broadband picker for real-time seismic monitoring and earthquake early-warning, Seism. Res. Lett., 83, 531–540, doi:10.1785/gssrl.83.3.531, 2012.

Lorito, S., Selva, J., Basili, R., Tiberti, M. M., and Piatanesi, A.: Probabilistic hazard for seismically induced tsunamis: accuracy and feasibility of inundation maps, Geophys. J. Int., 200, 574–588, doi:10.1093/gji/ggu408, 2015. 2917

Maramai, A., Brizuela, B., and Graziani, L.: The Euro-Mediterranean Tsunami Catalogue, Ann. Geophys.-Italy, 57, S0435, doi:10.4401/ag-6437, 2014. 2917

NEAMTWS: Interim Operational Users Guide for the Tsunami Early Warning and Mitigation System in the North-eastern Atlantic, the Mediterranean and Connected Seas (NEAMTWS), Version 2.0, ICG/NEAMTWS-VIII, edited by: Meyers, A., Springer, New York, 2011. 2916, 2929

Tsuboi, S., Takano, K. A., and Yamanaka, Y.: Rapid determination of M_w from broadband P waveforms, B. Seismol. Soc. Am., 85, 606–613, 1995. 2926, 2930, 2940

Tsuboi, S., Takano, K. A., and Yamanaka, Y.: Application of M_{wp} to deep and teleseismic earthquakes, B. Seismol. Soc. Am., 89, 1345–1351, 1999. 2940

Vassallo, M., Satriano, C., and Lomax, A.: Automatic picker developments and optimization: a strategy for improving the performances of automatic phase pickers, Seismol. Res. Lett., 83, 541–554, doi:10.1785/gssrl.83.3.541, 2012. 2919

Wessel, P. and Smith, W. H. F.: New version of the generic mapping tool released, EOS T. Am. Geophys. Un., Santander, Spain, 1995.

Whitmore, P. M., Tsuboi, S., Hirshorn, B., and Sokolowski, T. J.: Magnitude-dependent correction for Mwp, Science of Tsunami Hazards, 20, 187–192, 2002. 2925

Table 1. List of earthquakes occurred in the Mediterranean area located by Early-est with $M \geq 5.5$ between March 2012 and December 2014. For each event we listed the computed event origin time, epicenter coordinates, hypocenter depth and preferred magnitude (mb, M_{wp} or M_{wpd}), a reference magnitude, when the first Early-est location were available (in seconds after the event origin time) and when the magnitude stabilize in minutes after the first location available. The magnitude is stable when the difference with respect the final magnitude is $\leq \mp 0.1$.

Nr	Date	Time	lat.	lon.	Depth	Mag^{best}	Mag^{ref}	First loc.	First mag. stable
1	10 Jun 2012	12:44:15	36.36	28.93	19.7	$M_{wp} = 6.1$	$M_w^{CMT} = 6.1$	167 [s]	10 [min]
2	12 Sep 2012	03:27:43	34.77	24.08	10.0	mb = 5.7	$mb^{Nc} = 5.4$	201 [s]	7 [min]
3	8 Jan 2013	14:16:09	39.62	25.49	10.1	$M_{wp} = 5.7$	$M_w^{CMT} = 5.7$	174 [s]	3 [min]
4	15 Jun 2013	16:11:02	34.51	24.99	15.4	$M_{wp} = 6.4$	$M_w^{CMT} = 6.3$	181 [s]	2 [min]
5	16 Jun 2013	21:39:07	34.51	25.00	18.6	$M_{wp} = 6.1$	$M_w^{CMT} = 6.0$	117 [s]	3 [min]
6	12 Oct 2013	13:11:51	35.52	23.30	11.5	$M_{wp} = 6.6$	$M_w^{CMT} = 6.8$	194 [s]	2 [min]
7	28 Dec 2013	15:21:06	36.04	31.30	56.8	$M_{wp} = 6.0$	$M_w^{CMT} = 5.9$	358 [s]	5 [min]
8	26 Jan 2014	18:45:10	38.29	20.38	19.8	mb = 5.2	$M_w^{Nc} = 5.4$	115 [s]	3 [min]
9	3 Feb 2014	03:08:46	38.25	20.40	10.1	$M_{wp} = 6.1$	$M_w^{CMT} = 6.0$	77 [s]	7 [min]
10	4 Apr 2014	20:08:07	37.26	23.71	115.9	mb = 5.5	$M_w^{CMT} = 5.6$	119 [s]	6 [min]
11	24 May 2014	09:25:03	40.23	25.34	10.1	$M_{wp} = 6.6$	$M_w^{CMT} = 6.9$	124 [s]	7 [min]
12	29 Aug 2014	03:45:06	36.75	23.67	81.2	$M_{wp} = 5.8$	$M_w^{CMT} = 5.8$	119 [s]	4 [min]

Table 2. Global earthquake catalogs used for the analysis in this work. For each catalog we indicated the begin and end time of the time window of the dataset included into this work. Catalog abbreviation used into this paper is between brackets in the first column.

Catalog	Begin	End	type
Early-est (EEc)	Mar 2012	Dec 2014	automatic
Neic (Nc)	Jan 2004	Dec 2014	revised
Gfz (Gc)	Jun 2006	Dec 2014	revised
CSEM (Cc)	Oct 2004	Dec 2014	revised
PTWC (Pc)	28 Dec 2013	Jun 2014	revised
CMT-Harvard (CMT)	1976	010-2014	revised

Table 3. This table summarize the rules used by Early-est to define the *best magnitude* (i.e.: the most significative magnitude type) for each earthquake. Each location run Early-est computes mb, M_{wp}, M_{wpd}. The magnitude mb is computed using the 30 s time window or the apparent source time duration T_o as time window if $T_o < 30$ s and the IASPEI WWSSN-SP response for convolution. The magnitude M_{wp} is scaled to the largest of the first two maxima on integrated displacement within the window from t_P to $t_P + T_o$ time or 120 s after t_P, where t_P is the *P* arrival time, whichever window is the shortest. The magnitude M_{wpd} (*duration-amplitude*), which can be viewed as an extension of the M_{wp} moment-magnitude algorithm, is computed following the M_{wp} procedure and corrections described into Lomax and Michelini (2012).

Best magnitude	#[1]	Magnitude range[2]
M_{wpd}	≥ 6	$M_{wpd} \geq 7.2$
M_{wp}	≥ 6	$5.8 \leq M_{wp} < 7.2$
mb	≥ 6	$M_{wp} < 5.8$

[1]: Number of recording stations with good signal-to-noise ratio and reliable amplitude reading.
[2]: Magnitude range validity.

Table A1. Early-est parameter specifications.

Measure	References	Description, modifications
Td	(Lomax and Michelini, 2011)	Max. dominant period smoothed over 5 s in window from T_p to $T_p + 55$.
T_{50}Ex	(Lomax and Michelini, 2011)	T_{50} Excedance, modified as follow: 1. Reduced T_{50}Ex minimum distance to 5°.
Td·T_{50}Ex	(Lomax and Michelini, 2011)	Period-duration discriminant for tsunami potential, modified as follows: 1. Reduced Td·T_{50}Ex minimum distance to 5°.
T_o	(Lomax and Michelini, 2009a, b, 2011)	High-frequency, apparent source-duration, modified as follows: 1. Removed smoothing window width of 10 s from To for short durations:, applied with a linear ramp from 10 → 0 s for initial durations of 20 → 60 s, minimum duration is highest frequency in HF stream (0.2 s). 2. Reduced T_o minimum distance to 5°. 3. Added reference of T_o duration to *S* arrival time (T_s) if raw duration end time $T_{o,end}$ is after T_s (e.g. if $T_{o,end} > T_s + (T_s - T_p)/3$ then $T_o = T_{o,end} - T_s$).
mb(V_{max})	(Bormann and Saul, 2008, 2009)	mb body wave magnitude using V_{max} formulation: 1. Apply to BRB velocity a recursive, time-domain filter that implements the WWSSN-SP displacement response. 2. WWSSN-SP displacement response from Working Group on Magnitudes (Magnitude WG) of the International Association of Seismology and Physics of the Earth's Interior (IASPEI) Commission on Seismological Observation and Interpretation (CoSOI) 2011. This filter is applied to the BRB velocity, so effectively gives: integrate → simulate the WWSSN-SP response → differentiate, without doing the integration and differentiation. 1. Measure V_{max} – the peak from T_p to the lesser of $T_p + T_o$ or $T_p + 30$ s 2. Apply: $mb(V_{max}) = \log_{10}(V_{max}/2\pi) + Q(\Delta, h)$
M_{wp}	(Tsuboi et al., 1995, 1999)	M_{wp} magnitude, modified as follows: 1. Applied from T_p to the lesser of $T_p + T_o$ or $T_p + 120$ s.
M_{wpd}(RT)	(Lomax and Michelini, 2009a)	M_{wpd} duration-amplitude, large earthquake magnitude, modified as follows to allow simple and robust real-time application without event type determination: 1. Use constant $k = 4.213e19$; PREM depth correction; no geometrical spreading or attenuation corrections. 2. Moment correction applied to all event types if $T_o > 80$ s 3. Moment correction applied to all event types if $T_o > 80$ s 4. Reduced M_{wpd} minimum distance to 5° (Stable since added reference of T_o duration to T_s).
Focal mech.		*P* arrival, first-motion focal mechanism using the HASH program.
Focal mech.	(Hardebeck and Shearer, 2002)	Probabilistic, *P* arrival, first-motion and amplitude focal mechanism algorithm (fmamp). Uses oct-tree search; solution quality based on wighted distribution (quasi-pdf) of *P* and *T* axis. (Note: under development; not included yet in Early-est distribution.)

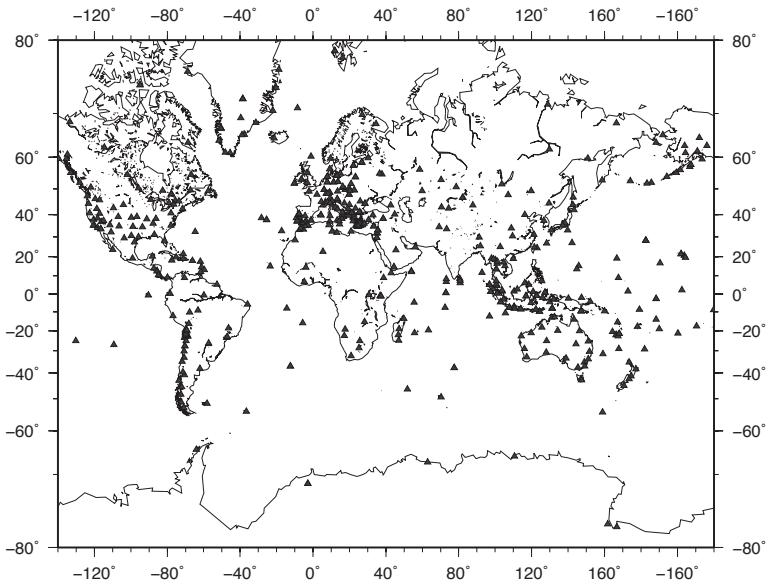

Figure 1. Global map with the 494 seismic broadband stations used by Early-est. The list is updated at the end of September 2014. The stations belong to the following networks: AK, AT, AU, BK, BL, CI, CN, CU, CX, CZ, DK, FR, GB, GE, GT, HL, HT, IC, II, IM, IN, IP, IU, IV, IW, JP, KZ, LB, LX, MN, MS, MY, ND, NN, NO, NZ, PL, PM, PS, SS, TM, TT, US, UW, WM. The network codes are assigned by the International Federation of Digital Seismograph Networks (FDSN) archive. When working in the real-time, latencies in the data stream and/or connection problems may occur, reducing the number of waveform available for location and magnitude estimation.

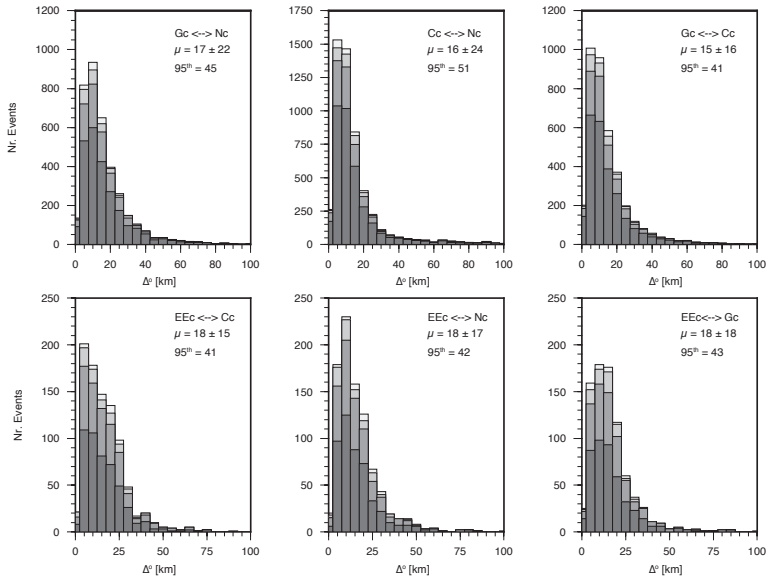

Figure 2. Epicenter location difference distributions for the events listed in the reference and in the Early-est catalogs. The epicenter location difference is expressed in km on the x axis; the vertical axis refers to the number of events for each bin; the bins are 5 [km] each. The top panels show the location difference between the locations of the three reference catalogs Nc, Gc, and Cc. The bottom panels show the location difference between Early-est and the reference catalogs. The gray color scale and magnitude ranges: dark grey $5.5 \leq M < 6$, middle dark grey $6.0 \leq M < 6.5$, middle light grey $6.5 \leq M < 7.0$, light grey. The mean and the SD and the 95 % percentiles for the entire dates (i.e. regardless to the magnitude) are indicated on the top right hand of each panel.

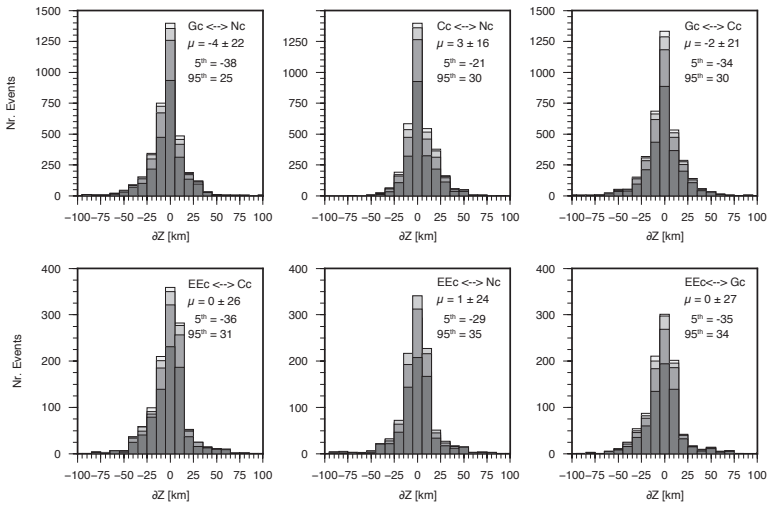

Figure 3. Hypocenter depth difference distributions for the events listed in the reference and in the Early-est catalogs. The hypocenter depth difference is expressed in km on the *x* axis; the vertical axis refers to the number of events for each bin; the bins are 5 [km] each. The top panels show the hypocenter depth difference distribution between the locations of the three reference catalogs Nc, Gc, and Cc. The bottom panels show the hypocenter depth difference between Early-est and the reference catalogs. The gray color scale and magnitude ranges: dark grey $5.5 \leq M < 6$, middle dark grey $6.0 \leq M < 6.5$, middle light grey $6.5 \leq M < 7.0$, light grey. The mean and the SD and the 95 % percentiles for the entire dates (i.e. regardless to the magnitude) are indicated on the top right hand of each panel.

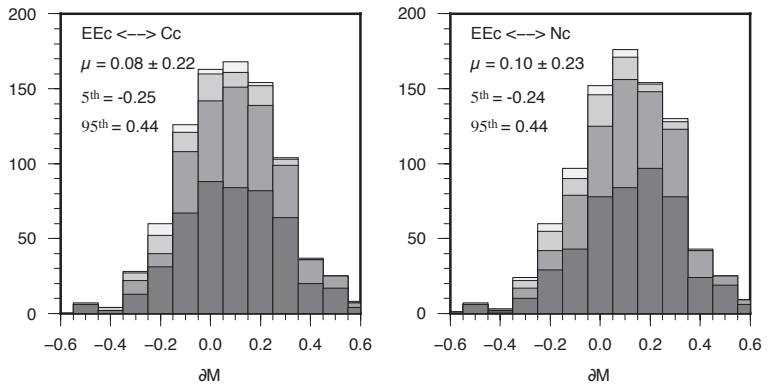

Figure 4. Magnitude difference distributions for the events listed in the EEc catalog with respect the two Ec and Cc reference catalogs. Differences are computed only when the same magnitude type is provided for the same event into the two compared catalogs. The magnitude difference is on the *x* axis; the vertical axis refers to the number of events for each bin; the bins are 0.1 magnitude each. The color scale refers to the same magnitude ranges as in Figs. 3 and 2 and not to the magnitude type. The gray color scale and magnitude ranges: dark grey $5.5 \leq M < 6$, middle dark grey $6.0 \leq M < 6.5$, middle light grey $M > 7.0\, 6.5 \leq M < 7.0$, light grey. The mean and the SD and the 95 % percentiles for the entire dates (i.e. regardless to the magnitude) are indicated on the top right hand of each panel.

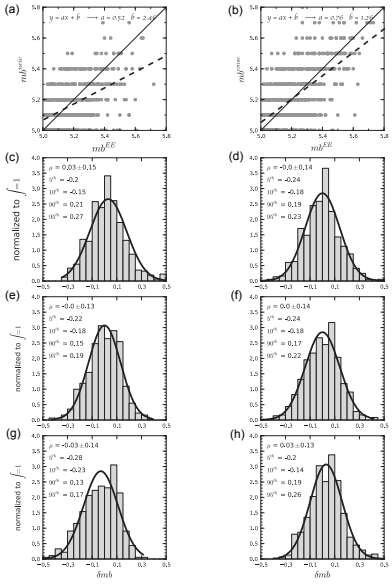

Figure 5. Magnitude mb differences between the Early-est catalog and the reference catalogs (Nc on the left and Cc on the right). Top row panels (**a** and **b**): magnitudes mb comparison between the Early-est values (*x* axis) and the reference catalog values (*y* axis). The dashed lines refer to the linear regression functions; the *a* and *b* constant are indicated on the left upper corner; the thin black line refers to the 1 : 1 proportion. 2nd row panels (**c** and **d**): magnitude mb difference distribution; the bins are 0.05 magnitude units wide each. The black line refers to the theoretical distribution derived from measured mean μ and SD σ with $\int = 1$. 3nd row panels (**e** and **f**): as in 2nd row panels but after applying the correction function showed in top panels to the Early-est mb. 4nd row panels (**g** and **h**): as in 3nd row panels, but on the left panel apply the EEc-Cc derived correction; on the right panel apply the EEc-Nc derived correction.

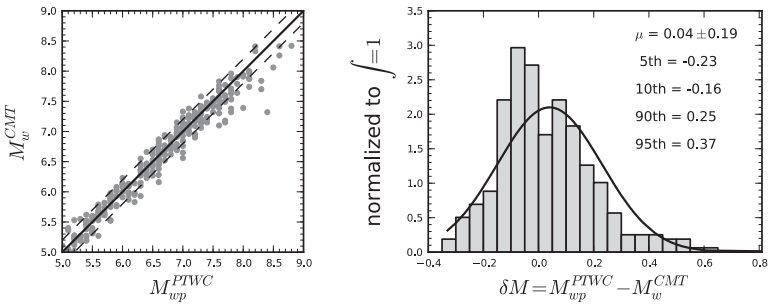

Figure 6. Comparison between the M_{wp} magnitudes computed by the Pacific Tsunami Warning Center (PTWC) with the M_w magnitudes from CMT-Harvard catalog. Plot on the left side: dot: magnitudes values; black line: 1 : 1 ratio; dashed lines: ∓0.2 uncertainty. The histogram on the right side show the $\delta M_{wp} - M_w$ distribution. Mean, SD and percentiles are indicated on the top right hand of the right panel. The bins are 0.05 magnitude wide each.

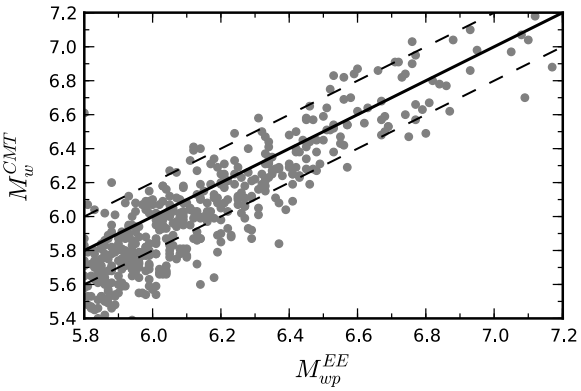

Figure 7. Early-est magnitudes M_{wp} compared with respect to Mw from the Global CMT catalog M_w of CMT-Harvard catalog. Black line: 1 : 1 ratio; dashed lines: ∓0.2 uncertainty.

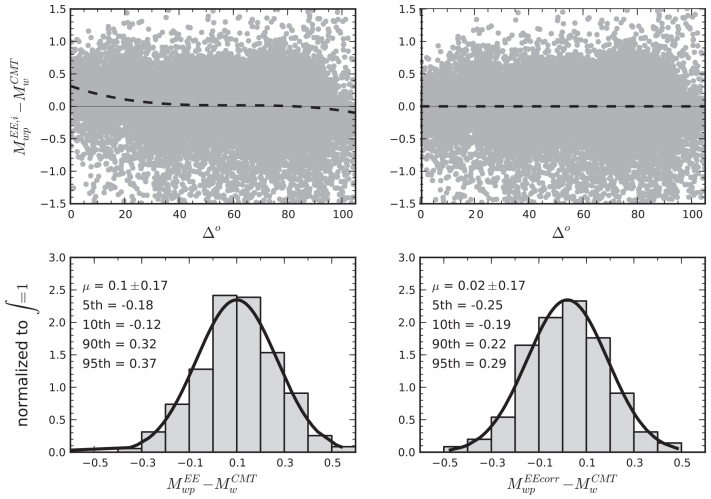

Figure 8. Epicentral distance dependence of the M_{wp} for events with hypocentral depth ≤ 100 [km]. Top left panel: station residuals $\delta M_{wp}^{i} = M_{wp}^{EE,i} - M_w^{CMT}$ (grey dots) plotted with respect the epicentral distance in degree; the dashed line represents a 3rd degree polynomial regression function (Eq. 1), which best fit the data. Top right panel: station residuals $\delta M_{wp}^{i} = M_{wp}^{EEcorr,i} - M_w^{CMT}$ (grey dots) after applying the regression function (Eq. 1), plotted with respect the epicentral distance in degree; the dashed line is a 3rd degree polynomial regression function, which fest fit the corrected residuals with respect the distance. Bottom left panel: event magnitude difference ΔM_{wp} distribution before the distance correction. These distribution reflect Fig. 7; mean, SD and percentiles are indicated on the left of the histogram; bins are 0.5 magnitude wide each; the black solid line refers to theoretical distribution with $\int = 1$. Bottom right panel: event magnitude difference ΔM_{wp}^{corr} distribution after the distance correction using Eq. (1).

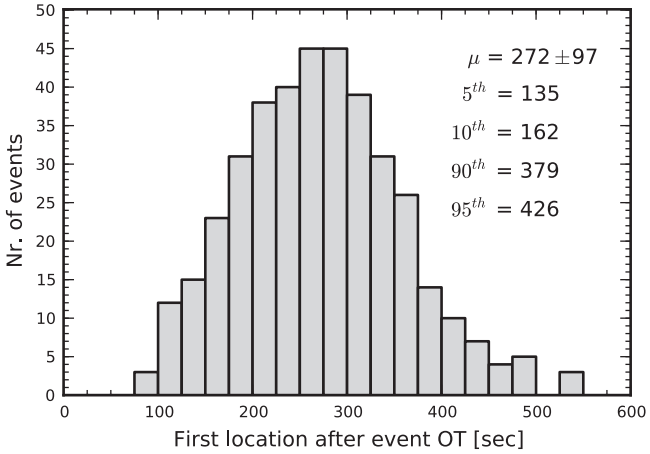

Figure 9. Early-est first location performance. This figure shows how fast a first location for global events is available through Early-est. The bins (25 s wide) on the *x* axis refers to the seconds after event origin time at which a first location is available. On the right top panel the mean, the SD and 4 representative percentiles are indicated.

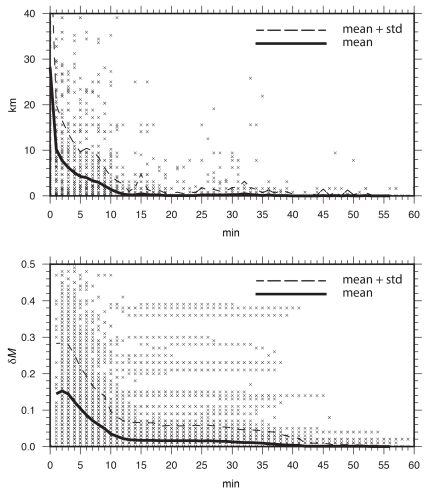

Figure 10. Early-est location and magnitude estimation stability performances. This figure shows how fast a first location (top panel) and magnitude (bottom panel) estimations stabilize towards the final values. Top panel: for each run we compute the distance in km between the current epicenter and the epicenter of the last location. Bottom panel: for each run we compute the absolute magnitude difference between the current magnitude and the final magnitude. In this panel, most of the magnitudes are available 2 min after event origin time, since often the first automatic location may not provide a magnitude value.The magnitude refers to the "best" magnitude decided by Early-est (Table 3) at each run. In both panels difference values (black cross) are plotted on the *y* axis with respect the minutes after the first location (0 value at the *x* axis). The black line is the mean value computed for each minute and the dashed line the mean plus the SD.

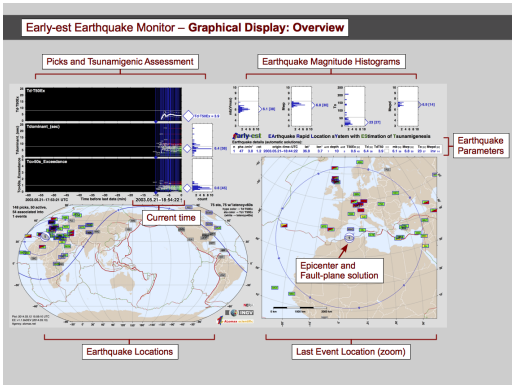

(a) Screen overview

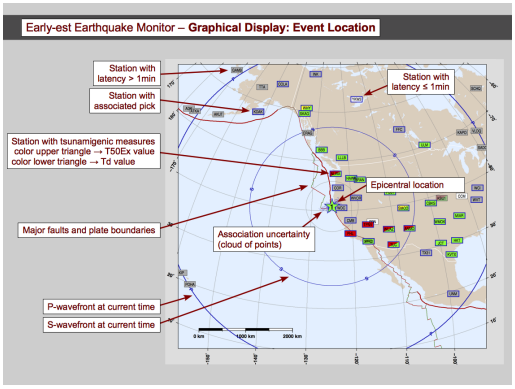

(b) Location map

Figure A1. Main graphical display of Early-est.

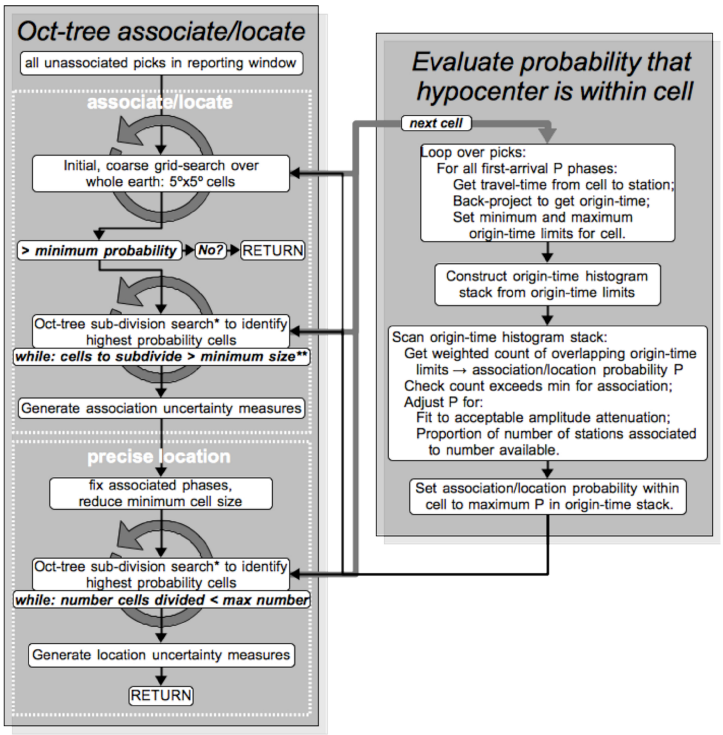

Figure A2. Early-est Associate/Locate Flow-Diagram: * Cell division is performed at a fixed cell size for a specified number of cells or until no cell available to divide; the fixed cell size is then reduced and cell division continued. ** Minimum size is adaptively reduced in proportion to number of associated stations near epicenter.